PAPER

Stability of topological properties of bismuth (1 1 1) bilayer

To cite this article: Maciej Bieniek *et al* 2017 *J. Phys.: Condens. Matter* **29** 155501

IOP Publishing Journal of Physics: Condensed Matter

J. Phys.: Condens. Matter **29** (2017) 155501 (9pp) https://doi.org/10.1088/1361-648X/aa5e79

Stability of topological properties of bismuth (1 1 1) bilayer

Maciej Bieniek, Tomasz Woźniak and Paweł Potasz

Department of Theoretical Physics, Wrocław University of Science and Technology, Wybrzeże Wyspiańskiego 27, 50-370 Wrocław, Poland

E-mail: maciej.bieniek@pwr.edu.pl

Received 7 December 2016, revised 20 January 2017
Accepted for publication 6 February 2017
Published 7 March 2017

Abstract

We investigate the electronic and transport properties of the bismuth (1 1 1) bilayer in the context of the stability of its topological properties against different perturbations. The effects of spin–orbit coupling variations, geometry relaxation and interaction with a substrate are considered. The transport properties are studied in the presence of Anderson disorder. Band structure calculations are performed within the multi-orbital tight-binding model and density functional theory methods. A band inversion process in the bismuth (1 1 1) infinite bilayer and an evolution of the edge state dispersion in ribbons as a function of spin–orbit coupling strength are analyzed. A significant change in the orbital composition of the conduction and valence bands is observed during a topological phase transition. The topological edge states are shown to be weakly affected by the effect of ribbon geometry relaxation. The interaction with a substrate is considered for narrow ribbons on top of another bismuth (1 1 1) bilayer. This corresponds to a weakly interacting case and the effect is similar to an external perpendicular electric field. Robust quantized conductance is observed when the Fermi energy lies within the energy gap, where only two counter-propagating edge states are present. For energies where the Fermi level crosses more in-gap states, scattering is possible between the channels lying close in the *k*-space. When the energy of the edge states overlaps the valence states, no topological protection is observed.

Keywords: bismuth, topological insulators, quantum transport

(Some figures may appear in colour only in the online journal)

1. Introduction

Topological insulators (TI) are bulk insulators which support protected boundary states [1–3]. In two-dimensional systems, this is manifested by the presence of helical 1D edge states, with the spin edge transport immune to non-magnetic disorder. This phenomenon is called the quantum spin Hall effect (QSHE), and was first noticed theoretically for graphene with spin–orbit interaction included [4]. This has stimulated a large body of research on both 2D and 3D materials. There are several experimentally confirmed 2D topological insulators, including CdTe/HgTe/CdTe [5] and AlSb/InAs/GaSb/AlSb [6] quantum wells, and $ZrTe_5$ [7, 8], Bi (110) [9] and Bi (1 1 1) bilayers [10–12], with many other systems predicted to support quantum spin Hall non-trivial states [13]. The list of experimentally addressed 3D topological insulators is even larger and constantly growing [14].

Topological protection against the backscattering of electrons transported through edge channels has been investigated by several authors [15, 16]. The situation is straightforward in cases when a pair of helical edge states linearly crosses the energy gap. Electrons propagating through edge channels are immune to backscattering due to spin-momentum locking. Since time reversal symmetry is present in the system, it is not possible to flip the spin and change the direction of movement. This leads to conductance quantization in disordered samples up to the point when disorder couples the edges of the system. On the other hand, an ideal situation with linearly dispersed edge states is not expected to occur in real systems. While topological insulators are characterized by an even number of

edge states crossing the energy gap, it is not clear whether deviation from linear dispersion affects topological protection against backscattering. Although the effect of scattering between the bulk and edge states has already been studied for both 2D [15, 16] and 3D TIs [17], the influence of extra in-gap states on transport is not well understood. The bismuth (1 1 1) bilayer was one of the first real-life systems predicted to be a 2D TI [18]. Free-standing bismuth bilayers have a 0.2 eV band gap at the Γ point, and it was shown that this can be further increased to 0.8 eV by the proper choice of substrate [19]. This makes Bi (1 1 1) highly compelling, as the gaps in other 2D TIs are of the order of meV. Calculations have shown the QSHE in Bi (1 1 1) to be stable against strain and electric fields [20], as well as choices of different substrates [21]. Compared to the Kane–Mele [4] and BHZ [22] models, the novel properties of edge states in ribbon geometry have been recognized [23], and a high level of tunability between the localized and extended edge states by chemical means has been predicted [24–32]. Orbital magnetization in quantum dot geometry resulting from edge state circulation has also been shown to exhibit similar robustness [33].

Despite intensive efforts to understand bismuth [34], some aspects of the topological properties of this material are still not clearly understood. Although the 3D Bi (1 1 1) crystal is conventionally known to be a trivial insulator (with the opposite possibility discussed by [35]), the non-trivial phase in thin films has been shown to survive up to four bilayers without even–odd oscillations [36]. The nature of the edge states measured recently [12] in the topmost layers of Bi (1 1 1) is also controversial ([37] and references therein). The problem of the robustness of the topological insulator phase in bismuth against different perturbations has also been studied within a limited scope [26, 32].

In this work, we focus on several aspects of the Bi (1 1 1) bilayer as a realistic model of the topological insulator. Using a combination of tight-binding and density functional theory methods, we study the effects of the spin–orbit coupling parameter, geometry relaxation and interaction with a substrate on the energy band structure. For 2D bismuth, a band inversion process as a function of spin–orbit coupling strength is examined. Ribbons are considered in two crystallographic orientations, with zigzag and armchair edges. We investigate changes in the dispersion of their edge states when perturbations and relaxation effects are included. Next, the transport properties in pure and disordered systems are studied. By controlling the Fermi energy position, we analyze the scattering processes between the edge and the ribbon valence band states. This allows us to distinguish the energy regimes with and without topological protection against backscattering. We also verify whether the topological Anderson insulator phase [38, 39] exists for ribbons within a trivial regime, in a similar way to CdTe/HgTe/CdTe systems.

2. Methodology

2.1. Lattice structure within density functional theory method

The Bi (1 1 1) bilayer is a buckled 2D honeycomb crystal, schematically shown in figure 1(a). A hexagonal unit cell contains two atoms and its geometrical parameters are: the lattice constant a and bilayer thickness h. We conducted the '*ab initio*' calculations with ABINIT software [40], which implements the density functional theory (DFT). The slabs of Bi bilayers and ribbons were separated by a vacuum region of 10 Å. The atoms were modeled within the frame of fully relativistic projector augmented waves (PAW) [41], and the general gradient approximation (GGA) of the exchange-correlation functional [42]. The structural parameters were optimized until the forces on the atoms were smaller than 10^{-7} Ha Bohr^{-}1. Monkhorst–Pack k-point grids of $8 \times 8 \times 1$ and $16 \times 16 \times 1$ were used for the structural optimization and density of states calculations, respectively. The plane wave basis cut-off was set to 20 Ha.

Our DFT calculations give the following values of structural parameters: the A–B atom distance along the z-axis $h = 1.73$ Å, and the A–A atom distance $a = 4.43$ Å. These are in good agreement with the calculations done by [43] ($h = 1.67$ Å for the isolated bilayer and $h = 1.65$ Å for the two bilayers), [21], correspondingly $h = 1.74$ Å and $a = 4.33$ Å, and the experimental values from [44] ($h = 1.64 \pm 0.04$ Å and $a = 4.39 \pm 0.05$ Å). These values differ from the parameters presented in [36] ($h = 1.58$ Å and $a = 4.52$ Å), although these calculations were performed with the use of the local density approximation, which is known to give different results from GGA for geometry optimization.

Besides the infinite Bi (1 1 1) bilayer plane, we studied the electronic properties of ribbons, which are structures with a finite width in a strip geometry periodic in one direction. We consider the two most stable edge terminations of a honeycomb lattice, namely the zigzag and armchair edge types. The width of the ribbon is determined by the number of atoms N_{at} in a direction perpendicular to the edge. We investigate the bismuth (1 1 1) bilayer ribbons with $N_{\mathrm{at}} = 90$ atoms, unless otherwise stated.

2.2. Tight-binding method

We use the four-orbital (s, p_x, p_y, p_z) tight-binding model (TB) developed by Liu and Allen [45] for bulk bismuth with a modification proposed by Murakami [18], in which all interlayer interactions are set to zero. The interatomic hopping up to the third nearest-neighbors and the atomic spin–orbit coupling (SOC) are parametrized with the Slater–Koster approach [46]. The Hamiltonian can be written as

$$
\begin{aligned}
H = & \sum_{i,\sigma,\vec{R}} \left(\left| i,\sigma,\vec{R} \right\rangle (E_i + U_i) \left\langle i,\sigma,\vec{R} \right| \right) \\
& + \sum_{i,j,\sigma,\vec{R},\vec{R}^{\mathrm{NN}}} \left(\left| i,\sigma,\vec{R} \right\rangle V_{ij}^{\mathrm{NN}} \left\langle j,\sigma,\vec{R}^{\mathrm{NN}} \right| + \mathrm{H.c.} \right) \\
& + \sum_{i,j,\sigma,\vec{R},\vec{R}^{\mathrm{NNN}}} \left(\left| i,\sigma,\vec{R} \right\rangle V_{ij}^{\mathrm{NNN}} \left\langle j,\sigma,\vec{R}^{\mathrm{NNN}} \right| + \mathrm{H.c.} \right) \\
& + \sum_{i,\sigma,\sigma',\vec{R}} \left(\left| i,\sigma,\vec{R} \right\rangle \frac{\lambda}{3} \vec{L} \cdot \vec{\sigma} \left\langle i,\sigma',\vec{R} \right| + \mathrm{H.c.} \right), \qquad (1)
\end{aligned}
$$

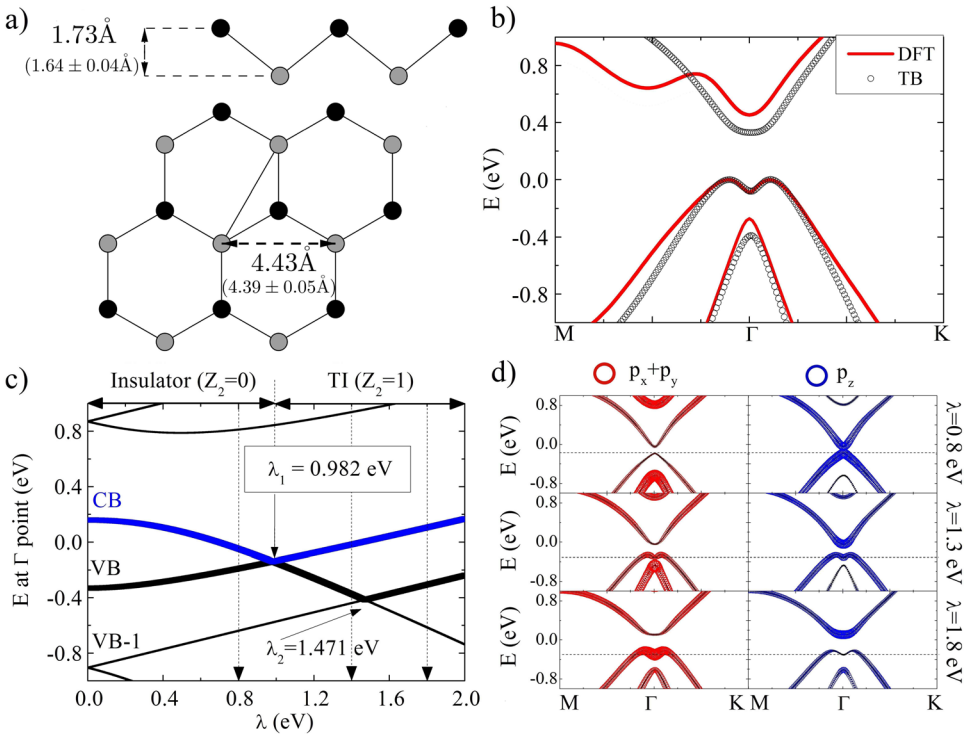

Figure 1. (a) The side and top view of the bismuth (1 1 1) structure with parameters obtained from the DFT calculations. The experimental values in brackets are taken from [44] and presented for comparison. (b) The energy band structure of the Bi (1 1 1) bilayer along the M-Γ-K direction obtained within the DFT (red lines) and TB methods (black circles) with the SOC $\lambda = 1.8$ eV. (c) The evolution of energies at the Γ point as a function of the SOC parameter λ using the TB method. A topological phase transition is observed for $\lambda_1 = 0.982$ eV. The second band crossing between the valence bands is seen for $\lambda_2 = 1.471$ eV. (d) The TB orbital composition for three different values of SOC parameter ($\lambda = 0.8, 1.3, 1.8$ eV); the radius of red (blue) dots represents the $p_x + p_y$ (p_z) orbital contribution to the bands.

where i, j indicate the $\{s, p_x, p_y, p_z\}$ orbitals and the $\{\sigma, \sigma'\}$ spins. $\vec{R}$ are the atomic positions with NN and NNN labeling the nearest and next-nearest neighbors, E_i denoting the on-site orbital energies and U_i representing an on-site random potential. V_{ij} are the Slater–Koster two-center integrals between the i and j orbitals. The last term corresponds to atomic SOC with λ as the SOC parameter. In our TB calculations, we first consider the SOC strength as a fitting parameter, and after comparison with the DFT results presented in the next section, we take $\lambda = 1.8$ eV. This value is slightly modified in comparison with Liu and Allen $\lambda = 1.5$ eV [45]. Thus, TB parametrization may lead to minor variations in the results, but they are all consistent in a qualitative way.

In the first term of the Hamiltonian given by equation (1), U_i is an on-site random potential with values chosen from the uniform distribution from $\left[-\frac{W}{2}, \frac{W}{2}\right]$. W denotes disorder strength and is implemented in order to study the transport properties in the presence of Anderson-type disorder. The conductance is studied as a function of the disorder strength, with the results averaged over 100 disorder realizations, which, as we verified, was sufficient to obtain reasonably small statistical fluctuations.

2.3. Transport calculations

For transport calculations, we consider two-terminal geometry with semi-infinite leads attached to the left and right edge of the scattering region. The Landauer formula for the differential conductance is given by

$$G = \frac{e^2}{h} T, \tag{2}$$

where T is the transmission coefficient between the left and right contacts, calculated using the recursive Green's functions method. T is calculated from

$$T = \mathrm{Tr}\left[\Gamma_L G^r_{1,N} \Gamma_R (G^r_{1,N})^\dagger\right] \tag{3}$$

where $G^r_{1,N}$ is a matrix representing the retarded Green's function between the first and the Nth slice, with the slicing procedure presented in [47] for zigzag and armchair graphene ribbons. $\Gamma_{L(R)}$ is defined as the difference between the semi-infinite lead self-energies ($\Gamma_{L(R)} = \Sigma_{L(R)} - \Sigma^\dagger_{L(R)}$), where the electron self-energies are calculated using the Sancho–Rubio [48] iterative algorithm. All calculations were performed for the non-interacting case and in $T = 0$ K. The semi-infinite leads, attached to the edges of the system, were considered as being made from the same material as the studied system to avoid the

contact resistance effect. We chose a system consisting of 90 by 180 bismuth atoms, which was sufficiently large to get size-independent results for the effects under consideration.

3. Energy band structure

3.1. Bi (1 1 1) *infinite bilayer*

The low-energy band structures of the Bi (1 1 1) bilayer along the M-Γ-K direction obtained with the DFT and TB methods are shown in figure 1(b). We observe a satisfying agreement between the TB model and DFT results close to the maximum of the valence band for the SOC parameter $\lambda = 1.8$ eV. The band structure has a well-defined energy gap at the Γ point. With the TB method, $E_{\mathrm{gap}} \approx 0.2$ eV, and an even larger gap ($E_{\mathrm{gap}} \approx 0.4$ eV) from the DFT calculations is obtained. We verified the non-trivial topology of the band structure by calculating the Z_2 invariant for inversion symmetric systems, according to the method from [49].

A band inversion point is determined by looking at the evolution of the valence band maximum and conduction band minimum as a function of the SOC parameter with the TB method [50], shown in figure 1(c). A topological phase transition is observed for $\lambda_1 = 0.982$ eV. A further increase in the SOC parameter leads to the second crossing within the valence bands at $\lambda_2 = 1.471$ eV, but it does not change the Z_2 invariant. The splitting between two valence bands—labeled as VB and VB − 1—depends crucially on the SOC strength (figure 1(c)). The choice of $\lambda = 1.8$ eV in our TB model with the band structure shown in figure 1(b) was motivated by fitting the VB to VB − 1 splitting to our DFT calculations.

The TB orbital composition of the low-energy band structure in a trivial phase for $\lambda = 0.8$ eV, the topological insulator phase before the second band crossing for $\lambda = 1.3$ eV, and the topological insulator phase after the second band crossing for $\lambda = 1.8$ eV, are shown in figure 1(d). For values of λ corresponding to the trivial phase, the low-energy bands are composed mostly of p_z orbitals. With an increase in SOC strength, the top of the valence band loses its p_z character and also becomes composed of $p_x + p_y$ orbitals. One can also note that with the variation of the SOC parameter, the character of band gap changes, from direct (in a trivial phase) to slightly indirect (figure 1(b)) after the topological phase transition. After the second band crossing for $\lambda_2 = 1.471$ eV, the p_z orbital contribution to the top of the valence band is further decreased.

3.2. Bi (1 1 1) *bilayer ribbons*

A characteristic feature of the electronic band structure of the topological insulators in strip geometry is the presence of counter-propagating edge states crossing the energy gap. We investigate the stability of these edge states against a variety of perturbations.

3.2.1. Spin–orbit coupling effect. While SOC is characterized by the type of material, it can be partially controlled by external factors like dopants or lattice curvature [51–53]. We would like to analyze how SOC strength affects the dispersion

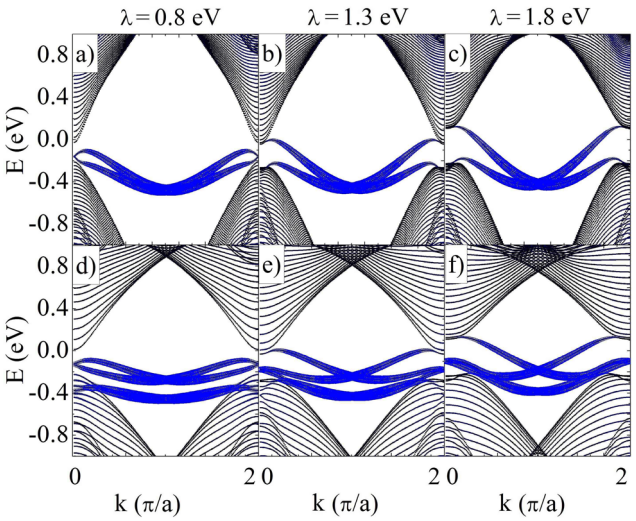

Figure 2. The energy band structures of zigzag ((a)–(c)) and armchair ((d)–(f)) bismuth ribbons with $N_{\mathrm{at}} = 90$ for three different values of SOC parameter, $\lambda = 0.8$ eV (a) and (d), $\lambda = 1.3$ eV (b) and (e), and $\lambda = 1.8$ eV (c) and (f), respectively. The thickness of the blue line represents the magnitude of the localization of states at two edge atomic sites. For $\lambda = 1.3$ eV and $\lambda = 1.8$ eV, in both the zigzag and armchair ribbons, there are edge states connecting the valence and conduction bands, which is a characteristic of topologically non-trivial states.

of the edge states. We consider wide ribbons to make the 1D band structure width-independent. This allows us to focus on the more general properties of the studied structures. In figure 2, the energy band structures for ribbons with $N_{\mathrm{at}} = 90$ and with zigzag (a)–(c) and armchair (d)–(f) edges are shown. We have considered three values of the SOC parameter (as in figure 1(d)): one representing a trivial phase for $\lambda = 0.8$ eV (a) and (d), the topological insulator phase before the second band crossing for $\lambda = 1.3$ eV (b) and (e), and the topological insulator phase after the second band crossing for $\lambda = 1.8$ eV (c) and (f). The size of the blue lines in figure 2 represents the magnitude of the localization of states at two atomic sites on both edges, showing that in-gap states are indeed localized almost solely on the boundaries of the ribbons.

First, we consider zigzag edge termination. For weak SOC $\lambda = 0.8$ eV within a trivial phase, two branches of edge states are attached to the top of the valence band at the boundaries of the Brillouin zone. Their dispersion is quasi-flat and they do not cross the energy gap (figure 2(a)). An increase in the SOC leads to a shift of the upper branch to the conduction band. After reaching a critical value of SOC, the upper branch of the edge states touches the conduction band at the boundaries of the Brillouin zone. We relate this to a topological phase transition after which the material becomes a TI. A further change in the SOC increases the energy band gap, which causes a larger dispersion of edge states, see figure 2(c). In the case of armchair ribbons, two branches of edge states are always present. For a weak SOC, one pair of edge states lies within the energy gap and the second pair has lower energy, overlapping with the valence band. Increasing the SOC affects the in-gap edge states more strongly, making them more dispersive. When a critical value of SOC is exceeded, they cross the energy gap connecting the valence and the conduction bands,

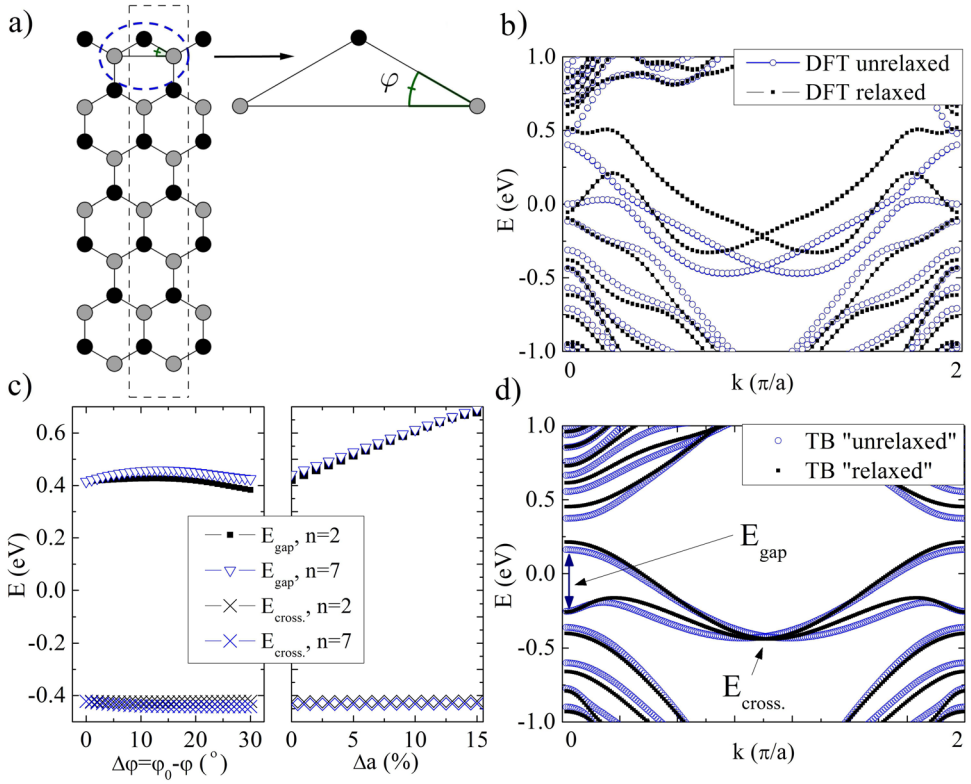

Figure 3. (a) A zigzag ribbon with $N_{at} = 14$; the unit cell is marked by a dashed rectangle. The angle φ parametrizes the position of an edge atom after relaxation. (b) The energy band structure of a relaxed and unrelaxed zigzag ribbon from the DFT method. (c) On the left: the energy band gap (E_{gap}) and the position of edge states crossing (E_{cross}) as a function of the angle deviation from the original value, $\Delta\varphi = \varphi_0 - \varphi$. Two values of $n = 2$ and $n = 7$ parametrize the variation of Slater–Koster integrals (see text) due to the bond shortening. On the right: an analogous analysis in the case of the variation of a lattice constant Δa for $\Delta\varphi = 5°$. (d) The band structures from the TB method of the relaxed and unrelaxed zigzag ribbon. The relaxed structure was modeled for $\Delta\phi = 10°$, $\Delta a = 1\%$ and $n = 7$.

in a similar way to the case of the zigzag ribbon. The lower branch of edge states remains attached to the top of the valence band and is not strongly affected by the change in SOC. Thus, we can assume that only one branch of the edge states has a topological origin, and the second one can be associated with trivial edge dangling bonds.

An interesting feature of the topological edge states in bismuth, in both types of ribbon edge termination, is that their dispersions depart from linearity, contrary to the clear Dirac-like spectrum in, e.g., the Kane–Mele model [4]. Close to the top of the valence band, one can notice a double crossing of the given Fermi energy by the edge state branch. The velocity direction of mobile electrons is determined by the dispersion relation $v \sim \delta E/\delta k$. Here, this quantity changes sign within the Brillouin zone for the edge states, which may affect the conductance due to possible scattering between counter-propagating states within a given edge. We come back to this issue in section 4.

3.2.2. Edge relaxation and substrate effect. The geometry relaxation of finite fragments of the ideal honeycomb lattice is a natural process related to the stabilization of structures, leading to the minimization of the total energy of the system. We investigate the band structure of a geometry-optimized zigzag ribbon with $N_{at} = 14$, see figure 3(a), performed in DFT ABINIT software, and compare it with the TB model with the modified edge hopping integrals. The relaxation mostly affects the edge lattice sites, which have only two neighbors, and the ideal edge hexagons are deformed. The edge atoms move towards the center of a hexagon, which decreases their relative distance to the two nearest-neighbors (by 0.04 Å) and changes the angle φ between atomic bonds from 30.00° to 28.41°, see figure 3(a). The effect of this shift has an influence on the energy band structure in the vicinity of the Fermi energy shown in figure 3(b) for the DFT results. The smooth edge states crossing the energy gap become slightly rippled, but the crossing remains. Thus, we do not expect the destruction of the topological properties of the system due to relaxation. We note here that small anti-crossings of the edge states after geometry relaxation for narrower ribbons occur, but the situation shown in figure 3(b) is more typical for wider ribbons.

Table 1. A list of non-zero Slater–Koster parameters for the edge atoms before and after relaxation (all values in eV). The modified values are given for $n = 7$, $\Delta\varphi = 10°$ and $\Delta a = 1\%$, which were used to obtain figure 3(d).

Parameter	Original value	Modified value
a	4.53	4.58
$V_{ss\sigma}$	−0.61	−0.92
$V_{sp\sigma}$	1.32	1.99
$V_{pp\sigma}$	1.85	2.79
$V_{pp\pi}$	−0.60	−0.90

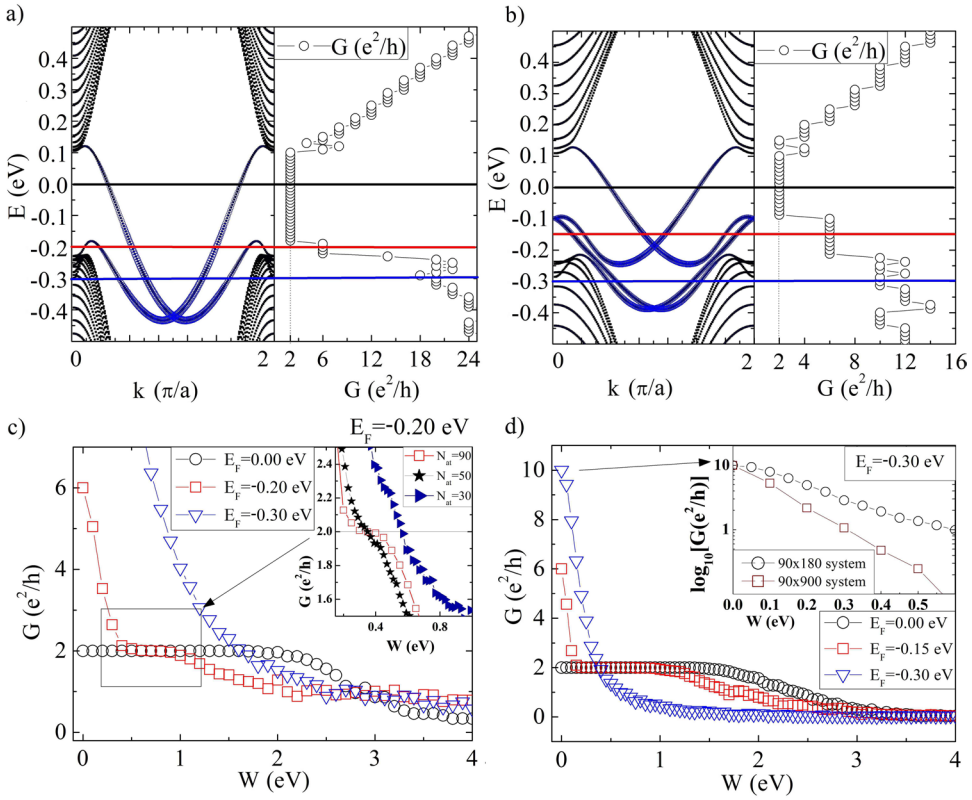

Figure 4. (a) and (b) The energy band structures (left) and transmission at a corresponding energy (right) for (a) zigzag and (b) armchair ribbons in a system without disorder. (c) and (d) The conductance of (c) zigzag and (d) armchair ribbons as a function of disorder strength W for three values of Fermi energies marked on (a) and (b) by horizontal colored lines. In the inset in (c) we present the results for different ribbon widths, $N_{at} = 30$, 50 and 90 atoms, keeping the aspect ratio of the system constant ($N_{width} = 2N_{at}$). The inset in (d) compares the decrease in the conductance as a result of the localization of states for energy below the top of the valence band for two different system lengths, with 180 and 900 atoms.

Next, we model the relaxation effect with the TB method by modifying the angles and hopping parameters between the edge atoms and their neighbors. The hopping parameters V_{ij} are changed according to Harrison theory [54], $V_{ij} = V^0_{ij}(d/d_0)^{-n}$, where V^0_{ij} are the original values of the Slater–Koster parameter, and d_0 and d are the original and modified bond lengths, respectively (see table 1). We take n as a parameter, which is responsible for the strength of V_{ij} modification due to bond shortening. The effect of edge modification on the band gap (E_{gap}) and the edge state crossing energy (E_{cross}) is presented in figure 3(c), where the angle ϕ (at the edges) and the lattice constant changes a (in the whole system) are studied. For both positive n and different φ, the band gap first increases and then after around $\Delta\varphi = 15^\circ$ starts to decrease. An increase in the lattice constant a leads to a wider band gap. Neither process affects the position of the edge state crossing in our TB model. We note that with the edge-modified TB model, figure 3(d), we were not able to change the dispersion of the edge states significantly, as seen in the DFT result in figure 3(b). This suggests that the mechanism of edge relaxation needs more sophisticated TB parametrization.

We also investigated the effect of a substrate on a narrow ($N_{at} = 14$) ribbon band structure. We considered a system which consists of two infinite bilayers, where periodic boundary conditions were imposed on the bottom one. We observe that two double degenerated branches of edge states split due to the inversion symmetry breaking (not shown here). This is a similar effect to an external perpendicular electric field when two sublattices of a honeycomb crystal become inequivalent [20]. We note here that such a situation is limited to a weakly interacting case, as the other type of substrate can interact more strongly with the ribbon, and the conclusions would not be valid anymore. Besides the degeneracy removal, no other significant effects were noticed for such a narrow ribbon. However, when the ribbon is wider, the energy gap decreases monotonically, vanishing for sizes around $N_{at} \sim 40$ atoms. In this case, the substrate is also expected to affect transport properties, as a contribution from the substrate states will be crucial.

4. Transport properties

The topological nature of the edge states ensures the protection against the backscattering of transported electrons. This is related to the helical edge channels, which results in spin-momentum locking. Electrons with a given spin traveling in one direction cannot be backscattered unless the spin-flip process occurs. As shown in a previous section, the edge state dispersion in bismuth ribbons is not linear, as in the simple TI model [4], and the velocity of the electron does not have a uniquely defined direction within the entire Brillouin zone. As the edge state dispersion allows the direction of movement to

be changed, it is tempting to verify whether backscattering in this case is still forbidden.

Figures 4(a) and (b) present the band structures and the corresponding conductance G at the given Fermi energy for zigzag and armchair ribbons with $N_{at} = 90$ atoms and in the absence of disorder. We consider three characteristic regimes of the Fermi energy position: within the band gap region with the edge states crossing the Fermi energy twice and six times, and below the energy gap, where the contribution to transport from the valence band states occurs, see the solid lines in figures 4(a) and (b). All states in the band structure are Kramers degenerate. When the sample is biased, each edge state results in a single contribution to the transport, increasing the conductance by e^2/h. The conductance within the first regime in the band gap region at the Fermi energy, represented by black lines in figures 4(a) and (b), is equal to $2e^2/h$. Then, it increases to $6e^2/h$ when the Fermi level is lowered, to the point where a double crossing occurs with the other branch of the edge states (red line). When the Fermi energy crosses more valence states, it starts to contribute to transport and one can observe an almost monotonic increase in the conductance. Deviations from this trend are seen for some energies and are attributed to unimportant size effects in the studied system.

For three characteristic regimes, we check how disorder influences the conductance of the system. We study samples with a scattering region composed of 90×180 atoms with semi-infinite pure leads attached at both ends. Anderson-type disorder is introduced by adding a random on-site potential to the lattice sites. When the Fermi level, represented by black lines in figures 4(a) and (b), crosses one pair of edge states, the transport is topologically protected, and only very strong disorder (above $W \approx 2$ eV) starts to localize the states. This results in decreasing conductance, see figure 4(c) for the zigzag and (d) for the armchair ribbons. In the zigzag ribbon, when the Fermi energy starts to cross the lower branch of edge states (the red line in figure 4(b)), we observe their fast localization, and as a consequence, a decrease in conductance from 6 to $2e^2/h$, marked with the red squares in figure 4(c). We explain this behavior as the scattering between two states from a lower branch of edge states near the boundaries of the Brillouin zone. Then, for disorder values between 0.4 and 0.9 eV, the conductance plateau is observed with $2e^2/h$, which is attributed to topologically protected transport through the states from an upper branch of the edge states. The inset shows that this only occurs for sufficiently wide samples. Further lowering of the Fermi energy, to the point where an overlap with the valence states is observed, causes edge state mixing and results in diminished conductance with respect to disorder strength. Similar effects are observed for an armchair ribbon. When the upper branch of the edge states starts to overlap with the lower one (the second regime), the conductance drops from 6 to $2e^2/h$—even more rapidly than in the zigzag ribbon. Interestingly, transport here is more stable compared to the zigzag case. The plateau is observed for $W \approx 0.2$ eV to $W \approx 1$ eV, however, this depends on the sample length (see the inset in 4(d)). When the edge states start to overlap the valence states, the quantized conductance is destroyed, just as in the zigzag case. We also note that when the ribbon is within a trivial insulator regime ($\lambda = 0.8$ eV),

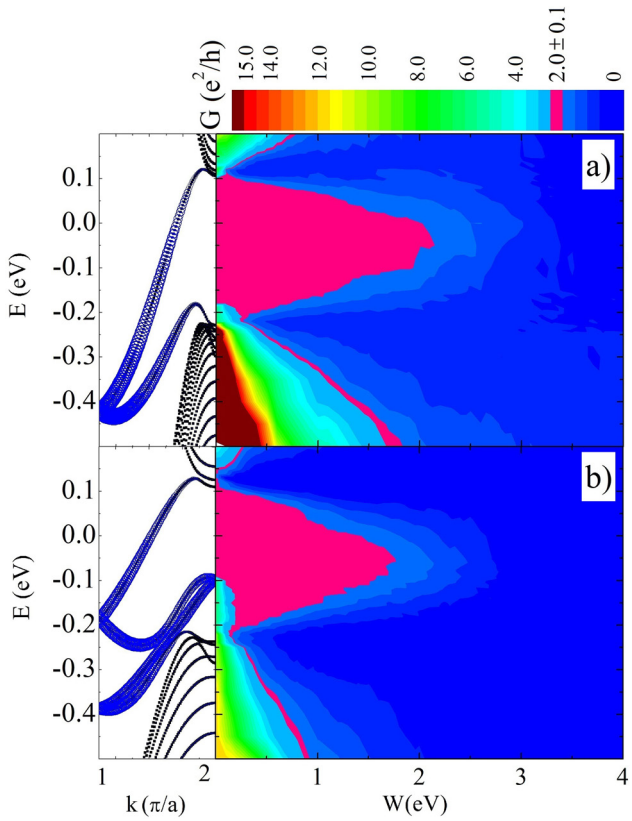

Figure 5. A map of the conductance G as a function of disorder strength W and the Fermi energy E for (a) zigzag and (b) armchair-type ribbons with 90×180 atoms. On the left we show the corresponding energy band structures for ribbons with $N_{at} = 90$. A region with topologically protected transport with $G = 2e^2/h$ is clearly visible.

we do not observe any signs of disorder-induced topological Anderson insulator phase [38, 39]. This is unexpected since in other models [38, 39, 55–57], TAI is induced by a diagonal type of disorder considered within this work. We also studied the effect of the substrate within the TI regime. We found that the splitting of states has no effect on the transport properties.

The results of the effects of disorder on the conductance are summarized in the maps shown in figures 5(a) and (b) for zigzag and armchair ribbons, respectively. In both cases, a large region within the energy gap with the quantized conductance $G = 2e^2/h$ is seen. In the armchair case within the energy region $E = (-0.1, -0.2)$, one can observe transport with the quantized conductance $G = 2e^2/h$, even when there are lower and upper edge state branches. Due to the short distance in reciprocal space between states from the lower branch, scattering within them is possible, which is not true for states from the upper branch. Thus, we conclude that the value of disorder strength necessary to break the ideally quantized conductance $G = 2e^2/h$ is affected by a distance between states in the k-space, and also an energetic distance between the valence and the edge states. Thus, this value does not depend on the level of localization of the wavefunction at the edge; see the localization of the edge states in figures 2(c) and (f). The conductance through the bulk states in the zigzag case is higher (dark red color in figure 5(a)), which is related to the larger density of states for this kind of edge termination.

5. Conclusions

In summary, we have studied the electronic and transport properties of the bismuth (1 1 1) bilayer and ribbons, in the context of the stability of their topological properties against different perturbations. We investigated the changes in energy band structures due to variations of SOC, the geometry relaxation effect and interaction with a substrate. We also studied the effects of Anderson-type disorder on the transport properties of this system. We varied the SOC parameter from the initial value $\lambda > 1.5$ eV, and we have shown that the system transforms into a trivial insulator for $\lambda < 0.982$ eV. In the bismuth (1 1 1) bilayer, this is associated with an inversion of bands in the energy band structure. In ribbons, the dispersion of the edge states flattens, and as a consequence, the connection between the valence and conduction bands of these states is destroyed. A change in the dispersion of the edge states associated with geometry relaxation has no effect on their topological nature. The effect of the interaction of a narrow ribbon with a substrate in the form of another bismuth bilayer is similar to that of an external perpendicular electric field. For the other type of substrate, or for wider ribbons, the coupling with the substrate is stronger. In such cases deeper studies are required.

In order to verify the topological protection of the edge states against backscattering, we examined the transport properties in the presence of Anderson-type disorder. We have shown a regime with the quantized conductance unaffected by weak disorder, where the edge states have a quasi-linear dispersion within the energy band gap. We also note that within this regime no effect of the interaction with a substrate can be noticed. For energies where an edge state crosses the given Fermi energy twice (zigzag ribbon case), or there are two branches of edge states (armchair ribbon case), scattering is possible between channels lying close in the k-space. In this case, transport through the edge channels localized in a different part of the Brillouin zone was still unaffected by weak disorder. When the Fermi energy overlaps the valence state energies, no topological protection is noticed. We have also verified that the TAI phase does not appear in bismuth when the SOC is decreased, changing the system into a trivial insulator.

Acknowledgments

The authors acknowledge partial financial support from the National Science Center (NCN), Poland, grant Sonata no. 2013/11/D/ST3/02703. Our calculations were performed in the Wrocław Center for Networking and Supercomputing. We also acknowledge the assistance of M Brzezińska and P Scharoch in editing the manuscript.

References

[1] Moore J 2010 *Nature* **464** 194
[2] Hasan M Z and Kane C L 2010 *Rev. Mod. Phys.* **82** 3045
[3] Qi X L and Zhang S C 2011 *Rev. Mod. Phys.* **83** 1057
[4] Kane C L and Mele E J 2005 *Phys. Rev. Lett.* **95** 226801
[5] König M, Wiedmann S, Brüne C, Roth A, Buhmann H, Molenkamp L W, Qi X L and Zhang S C 2007 *Science* **318** 766
[6] Knez I, Du R R and Sullivan G 2011 *Phys. Rev. Lett.* **107** 136603
[7] Li X B *et al* 2016 *Phys. Rev. Lett.* **116** 176803
[8] Wu R *et al* 2016 *Phys. Rev.* X **6** 021017
[9] Lu Y *et al* 2015 *Nano Lett.* **15** 80
[10] Yang F *et al* 2012 *Phys. Rev. Lett.* **109** 016801
[11] Sabater C, Gosálbez-Martínez D, Fernández-Rossier J, Rodrigo J G, Untiedt C and Palacios J J 2013 *Phys. Rev. Lett.* **110** 176802
[12] Drozdov I K, Alexandradinata A, Jeon S, Nadj-Perge S, Ji H, Cava R J, Bernevig B A and Yazdani A 2014 *Nat. Phys.* **10** 664
[13] Ren Y, Qiao Z and Niu Q 2016 *Rep. Prog. Phys.* **79** 066501
[14] Ando Y 2013 *J. Phys. Soc. Japan* **82** 102001
[15] Zhang Y Y, Shen M, An X T, Sun Q F, Xie X C, Chang K and Li S S 2014 *Phys. Rev.* B **90** 054205
[16] Baum Y, Posske T, Fulga I C, Trauzettel B and Stern A 2015 *Phys. Rev. Lett.* **114** 136801
[17] Saha K and Garate I 2014 *Phys. Rev.* B **90** 245418
[18] Murakami S 2006 *Phys. Rev. Lett.* **97** 236805
[19] Zhou M, Ming W, Liu Z, Wang Z, Li P and Liu F 2014 *Proc. Natl Acad. Sci.* **111** 14378
[20] Chen L, Wang Z F and Liu F 2013 *Phys. Rev.* B **87** 235420
[21] Huang Z Q, Chuang F C, Hsu C H, Liu Y T, Chang H R, Lin H and Bansil A 2013 *Phys. Rev.* B **88** 165301
[22] Bernevig B A, Hughes T L and Zhang S C 2006 *Science* **314** 1757
[23] Wada M, Murakami S, Freimuth F and Bihlmayer G 2011 *Phys. Rev.* B **83** 121310
[24] Chen L, Cui G, Zhang P, Wang X, Liu H and Wang D 2014 *Phys. Chem. Chem. Phys.* **16** 17206
[25] Jin K H and Jhi S H 2014 *Sci. Rep.* **5** 8426
[26] Jin K H and Jhi S H 2016 *Phys. Chem. Chem. Phys.* **18** 8637
[27] Ma Y, Dai Y, Kou L, Frauenheim T and Heine T 2015 *Nano Lett.* **15** 1083
[28] Ma Y, Li X, Kou L, Yan B, Niu C, Dai Y and Heine T 2015 *Phys. Rev.* B **91** 235306
[29] Niu C, Bihlmayer G, Zhang H, Wortmann D, Blügel S and Mokrousov Y 2015 *Phys. Rev.* B **91** 041303
[30] Wang Z F, Chen L and Liu F 2014 *Nano Lett.* **14** 2879
[31] Wang D, Chen L, Liu H, Wang X, Cui G, Zhang P, Zhao D and Ji S 2015 *Phys. Chem. Chem. Phys.* **17** 3577
[32] Li X, Liu H, Jiang H, Wang F and Feng J 2014 *Phys. Rev.* B **90** 165412
[33] Potasz P and Fernández-Rossier J 2015 *Nano Lett.* **15** 5799
[34] Hofmann P 2006 *Prog. Surf. Sci.* **81** 191
[35] Ohtsubo Y, Perfetti L, Goerbig M O, Fvre P L, Bertran F and Taleb-Ibrahimi A 2013 *New J. Phys.* **15** 033041
[36] Liu Z, Liu C X, Wu Y S, Duan W H, Liu F and Wu J 2011 *Phys. Rev. Lett.* **107** 136805
[37] Yeom H W, Jin K H and Jhi S H 2016 *Phys. Rev.* B **93** 075435
[38] Li J, Chu R L, Jain J K and Shen S Q 2009 *Phys. Rev. Lett.* **102** 136806
[39] Groth C W, Wimmer M, Akhmerov A R, Tworzydło J and Beenakker C W J 2009 *Phys. Rev. Lett.* **103** 196805
[40] Gonze X *et al* 2009 *Comput. Phys. Commun.* **180** 2582
[41] Holzwarth N, Tackett A and Matthews G 2001 *Comput. Phys. Commun.* **135** 329
[42] Perdew J P, Burke K and Ernzerhof M 1996 *Phys. Rev. Lett.* **77** 3865
[43] Koroteev Y M, Bihlmayer G, Chulkov E V and Blügel S 2008 *Phys. Rev.* B **77** 045428
[44] Hirahara T, Fukui N, Shirasawa T, Yamada M, Aitani M, Miyazaki H, Matsunami M, Kimura S, Takahashi T,

Hasegawa S and Kobayashi K 2012 *Phys. Rev. Lett.* **109** 227401
[45] Liu Y and Allen R E 1995 *Phys. Rev.* B **52** 1566
[46] Slater J C and Koster G F 1954 *Phys. Rev.* **94** 1498
[47] Lewenkopf C H and Mucciolo E R 2013 *J. Comput. Electron.* **12** 203
[48] Lopez-Sancho M P, Lopez-Sancho J M and Rubio J 1985 *J. Phys. F: Met. Phys.* **15** 851
[49] Fu L and Kane C L 2007 *Phys. Rev.* B **76** 045302
[50] Bieniek M, Woźniak T and Potasz P 2016 *Acta Phys. Pol.* **130** 609
[51] Han W, Kawakami R K, Gmitra M and Fabian J 2014 *Nat. Nano.* **9** 794
[52] Fratini S, Gosálbez-Martínez D, Merodio Cámara P and Fernández-Rossier J 2013 *Phys. Rev.* B **88** 115426
[53] Huertas-Hernando D, Guinea F and Brataas A 2006 *Phys. Rev.* B **74** 155426
[54] Harrison W A 1980 *Electronic Structure and the Properties of Solids* 1st edn (New York: Dover)
[55] Jiang H, Wang L, Sun Q F and Xie X C 2009 *Phys. Rev.* B **80** 165316
[56] Song J, Liu H, Jiang H, Sun Q F and Xie X C 2012 *Phys. Rev.* B **85** 195125
[57] Lv S H, Song J and Li Y X 2013 *J. Appl. Phys.* **114** 183710